Available online at www.sciencedirect.com
SCIENCE DIRECT®
International Journal of Pharmaceutics 277 (2004) 39–61
international journal of pharmaceutics
www.elsevier.com/locate/ijpharm

Tumor targeting based on the effect of enhanced permeability and retention (EPR) and the mechanism of receptor-mediated endocytosis (RME)

T. Tanaka*, S. Shiramoto, M. Miyashita, Y. Fujishima, Y. Kaneo

Department of Biopharmaceutics, Faculty of Pharmacy and Pharmaceutical Sciences, Fukuyama University, 1 Gakuen-cho, Fukuyama, Hiroshima 729-0292, Japan

Received 1 August 2002; received in revised form 26 December 2002; accepted 19 September 2003

Available online 9 April 2004

Abstract

This review is focused on the macromolecular drug carrier systems by the effect of enhanced permeability and retention (EPR) and the mechanism of receptor-mediated endocytosis (RME). The effect of EPR is thought to be useful for the targeting of the macromolecular drugs to the tumor tissues on a vasculolymphatic level. The RME reveals the selective recognition, high affinity binding, and immediate internalization for the ligand on a cellular level. In the receptor, recognizing transferrin, a level of expression on the tumor cells is higher than that on the normal cells. We have used serum albumin and transferrin as drug carriers to deliver mitomycin C (MMC) to the tumor tissues and into the tumor cells. The properties of the conjugates of MMC to serum albumin and transferrin were examined in vitro and in vivo. We concluded that MMC could be delivered to the tumor tissue and cells by the use of albumin and transferrin as drug carriers.

Keywords: Drug delivery system; Tumor targeting; Mitomycin C; Macromolecular conjugate; Serum albumin; Transferrin; Enhanced permeability and retention; Receptor-mediated endocytosis; Intracellular disposition; Antitumor activity

1. Targeting based on the effect of EPR

1.1. Introduction

Macromolecular carrier systems have been developed in an attempt to optimize the delivery of antineoplastic agents. The idea behind use of drug-macromolecule conjugates is that they may show improvement in the distribution of the drug (Friend and Pangburn, 1987). Mitomycin C (MMC) has the potential to act against a number of human neoplasms. However, it presents the problems of severe myelosuprression and gastrointestinal complications. A variety of macromolecular conjugates of MMC have been demonstrated in vitro and in vivo, e.g., antibodies (Manabe et al., 1985), glycoprotein (Kaneo et al., 1991), albumin (Kato et al., 1983), dextran (Hashida et al., 1983), and synthetic macromolecules such as polylysine (Roos et al., 1984). Approaches that take advantage of antibodies show some potential for achieving active targeting, such as HERCEPTIN (trastuzumab) and RITUXAN (rituximab). On the other hand, a process of passive targeting utilizes the natural distribution pattern of the macromolecular and particulate carrier to deliver the drug to the specific site of action. SMANCS (zinostatin stimalamer) and

* Corresponding author. Tel.: +81-849-36-2111; fax: +81-849-36-2024.
E-mail address: tanaka@fupharm.fukuyama-u.ac.jp (T. Tanaka).

0378-5173/$ – see front matter © 2004 Elsevier B.V. All rights reserved.
doi:10.1016/j.ijpharm.2003.09.050

DOXIL (doxorubicin HCl liposome injection) are divided into the passive targeting drug.

Macromolecules such as albumin, globulins, and synthetic polymer accumulate in the tumor tissues because these tissues have a vascular network characterized by both enhanced permeability of the neovasculature and a lack of the lymphatic recovery system (Matsumura and Maeda, 1986). These findings led us to inquire whether MMC might accumulate in the tumor tissues by the use of albumin-conjugate system.

We have previously described the covalent attachment of MMC to serum albumin to give MMC-albumin conjugates which aided the tumor localization of MMC (Kaneo et al., 1990). Physicochemical properties of macromolecular carriers such as size and electric charge influence the biological properties of the macromolecular conjugate and hence require careful consideration (Takakura et al., 1987; Roos et al., 1984). At the present stage of the investigation of MMC-albumin conjugates, little is known about these physicochemical and biological properties. In this section, we describe the methods to prepare MMC-albumin conjugates in which MMC is covalently attached to albumin through a glutaryl group spacer. The physicochemical properties of these conjugates, such as degree of chemical modification, molecular weight and size, α-helical content, and release of MMC, are listed, together with preliminary examinations of their biological behavior, such as antitumor activity, toxicity and tumor localization, in animals (Tanaka et al., 1991).

1.2. Materials and methods

1.2.1. Materials

Bovine serum albumin (BSA) (fraction V, Sigma Chemical Co., St. Louis, MO, USA) was further purified by gel filtration on Sephadex G-150. Glutaric anhydride, MMC, *N*-hydroxysuccinimide, 1-ethyl-3-[3-(dimethylamino)propyl]carbodiimide hydrochloride (EDC), tetra-*n*-butylammonium bromide (TBAB) and 2,4,6-trinitrobenzenesulfonic acid sodium salt (TNBS) were obtained from Nacalai Tesque, Inc. (Kyoto, Japan). Gel filtration calibration kits and molecular weight electrophoresis calibration kits were obtained from Pharmacia Fine Chemicals (Uppsala, Sweden). All other chemicals were of analytical grade or the best quality available.

1.2.2. Preparation of albumin conjugates of MMC

MMC was covalently attached to BSA through a glutaryl group spacer by the following methods (Tanaka et al., 1991).

1.2.2.1. Method 1. BSA was glutarylated before the conjugation of MMC. EDC was added to the reaction mixture of glutarylated BSA (G-BSA) and MMC. The conjugate of G-BSA and MMC (G-BSA-MMC) was purified by gel filtration and lyophilized.

1.2.2.2. Method 2. After glutarylation of MMC, *N*-hydoxysuccinimide was used to produce an active ester. BSA was reacted with the active ester to prepare a conjugate of glutarylated MMC with BSA (BSA-G-MMC). The conjugate was purified by gel filtration and lyophilized.

1.2.3. Determination of both contents of MMC and amino groups

The MMC content of the conjugate was calculated from the UV absorbance at 363 nm in 0.9% NaCl with reference to the absorbance rate of the MMC standard. The protein content of the conjugate was determined by the method of Lowry with a BSA standard. The MMC content of the conjugate was calculated by dividing the content of MMC by that of protein.

Free amino groups were determined according to the method of Fields (1972). The sample solution was diluted with absorbate buffer. Then, a solution of 0.11 M TNBS was added. After exactly 5 min, the reaction was stopped by addition of 0.1 M NaH_2PO_4 containing 1.5 mM Na_2SO_3. The absorption at 420 nm was correlated with the number of free amino groups.

1.2.4. Size-exclusion chromatography

The sample dissolved in 0.2 M NaCl was applied on a column (1.0 cm × 47 cm) of Sephadex G-150. The mobile phase was 0.2 M NaCl, and the flow rate was 17.1 ml/h. The absorbance of the eluted solution was monitored at 280 and 363 nm. The Stokes radius of the conjugate was determined by the calibration curve with four kinds of standard proteins.

1.2.5. Gel electrophoresis

Sodium dodecyl sulfate polyacrylamide gel electrophoresis (SDS–PAGE) was performed according to the method of Laemmli (1970). A separating gel (7 cm

long) containing 10% acrylamide was used in combination with a stacking gel (1 cm long, 4.5% acrylamide). Electrophoresis was carried out with a current of 20 mA per 8 cm width of the gel. After electrophoresis, the protein bands were visualized by staining with Coomassie Brilliant Blue. The molecular weight of the conjugate was estimated by the calibration curve with standard proteins.

1.2.6. Estimation of helical content

Circular dichroism (CD) spectra were recorded on a JASCO J-20C spectropolarimeter equipped with a J-DPZ data processor (Japan Spectroscopic Co. Ltd., Tokyo, Japan) using a 0.1 mm thick cuvette at room temperature ($25 \pm 3\,^{\circ}C$) under constant nitrogen flush. The spectropolarimeter was calibrated by using androsterone, and each spectrum was the result of four or more accumulations. The helical content of the conjugate was estimated according to the method of Chang and Sun (1978).

1.2.7. Stability experiments

The release of MMC and G-MMC from the conjugate was determined in a 0.1 M phosphate buffer system (pH 5.0, 6.0, 7.4, 8.0, and 9.0, $\mu = 0.3$) at 37 °C according to the method of Hashida et al. (1983). The experiment was initiated by dissolving the conjugate in a preheated buffer solution to produce a concentration of 10 mg/ml. At a fixed time interval, the amounts of MMC and G-MMC released were determined simultaneously by using an HPLC method described later. The stability of MMC and the conjugates was also measured photometrically under the same conditions.

1.2.8. Animals and tumor cells

Male Wistar rats (190–210 g) and male ddY mice (20–30 g) were obtained from Japan SLC, Inc. (Shizuoka, Japan). Ehrlich ascites carcinoma (EAC) and Sarcoma 180 (S180) cells were kindly supplied by Dr. Sato (Sasaki Laboratory, Tokyo, Japan) and maintained in ddY mice by weekly intraperitoneal transplantation.

1.2.9. Pharmacokinetics in rats

Rats fasted for 24 h were anesthetized with sodium pentobarbital (40 mg, i.p. injection). The femoral artery was cannulated with polyethylene tubing (PE-50). The conjugate (0.5 mg/kg in MMC equivalents) or MMC (1 mg/kg) in 0.2 ml of 0.9% NaCl was injected through the jugular vein. Blood was collected periodically from the femoral artery after the injection. Plasma concentration of MMC was determined with a HPLC described later.

1.2.10. Tissue distribution in tumor-bearing mice

EAC cells (1×10^6 cells/mouse) were inoculated into the subcutaneous tissue of the axillary region of ddY mice. Fourteen days after the inoculation, the EAC-bearing mice were administered the conjugate (20 mg/kg in MMC equivalents) intravenously through the tall vein. After 24 h, the blood was collected from the vena cava under ether anesthesia and the tumor tissue, liver, spleen, kidney, lung, heart, intestine, and muscle were excised and weighed. Tissue levels of MMC were determined by using an HPLC method.

1.2.11. In vivo antitumor activity

Inhibitory effect of the conjugate on the growth of S180 was studied according to the procedure of Takakura et al. (1987). S180 cells (1×10^7 cells/mouse) were inoculated into the subcutaneous tissue of the axillary region of ddY mice. Four days after the inoculation, a single intravenous dose of the conjugate (20 mg/kg in MMC equivalents) or MMC (5 mg/kg) dissolved in 0.9% NaCl was administered to the tumor-bearing mice. Tumor sizes were measured with calipers, and the tumor volumes were calculated. The tumor growth was monitored by the increasing rate of the tumor volume after the inoculation.

1.2.12. Acute toxicity in mice

Toxicities of the conjugates and MMC were evaluated with the survival on the seventh day after the intravenous single injection of the test compound to male ddY mice. LD_{50} values were determined according to Dixon (1965). The mice were permitted access to food and water ad libitum. By the up-and-down protocol, mice were observed for 7 days after dosing.

1.2.13. Analytical method

The amounts of MMC and G-MMC released from the conjugate in vitro were determined simultaneously by HPLC. The chromatographic system (LC-6A, Shimadzu, Kyoto, Japan) with a variable-wavelength UV detector (SPD-6A) operated at 350 nm. A 4.6 mm × 250 mm, C_{18} reversed-phase column (TSK

Table 1
Physicochemical properties of G-BSA-MMC and BSA-G-MMC

	G-BSA-MMC	BSA-G-MMC	G-BSA	BSA
MMC content				
MMC/w (%)	6.03 ± 0.92	2.82 ± 0.51		
Molar ratio	12.1 ± 1.8	5.59 ± 1.00		
Free amino residue[a] (mol)	1.5 ± 0.5	22.9 ± 14	1.2 ± 0.4	28.5 ± 0.8
Effective molecular size[b] (Å)	45.1	36.6	45.5	34.4
Apparent molecular weight[c] (kDa)	84	73	94	68
Helical content[d] (%)	32.2 ± 3.3	50 ± 0.3	30.1 ± 44	51.6 ± 1.3

[a] Free amino groups were determined by the method of TNBS.
[b] Effective molecular sizes were determined by a size-exclusion chromatography.
[c] The apparent molecular weights were determined by SDS–PAGE.
[d] Helical contents were estimated by the measurement of CD according to the method of Chang and Sun (1978).

gel 120T, Tosoh, Tokyo, Japan) was used at ambient temperature. The mobile phase was 20% acetonitrile in 40 mM phosphate buffer (pH 7.0) containing 2.5 nM TBAB as an ion-pairing agent and the flow rate was 1.0 ml/min. It was confirmed that the determination of both MMC and G-MMC was not affected by the presence of the conjugate, and neither MMC nor G-MMC was liberated from the conjugate during the determination process. The concentration of MMC in plasma and tissue was determined as follows. Blood was centrifuged at 8000 × *g* for 30 s to obtain a plasma sample. The excised tissues were homogenized (25%) in 0.1 M phosphate buffer (pH 74). The plasma samples and the tissue homogenates were assayed according to the procedures of Hashida et al. (1983).

1.3. Results

1.3.1. Preparation of mitomycin C-albumin conjugates

Two types of MMC-albumin conjugates, namely, G-BSA-MMC and BSA-G-MMC, were synthesized. Both MMC-albumin conjugates showed an absorbance which contains the pattern of free MMC between 300 and 400 nm, while the precursors themselves showed no UV absorption in this range.

Physicochemical properties of the conjugates are summarized in Table 1. The MMC contents of G-BSA-MMC and BSA-G-MMC were 6.0 and 2.8 w/w (%), respectively, corresponding to 12.1 and 5.6 mol of MMC/mol of BSA. One mole of BSA showed the color intensity of 28.5 mol of free amino groups with reference to the molar absorptivity of epsilon-amino groups of lysine (13,300 M^{-1} cm^{-1}). On the BSA-G-MMC molecule, 22.9 mol free amino groups were detected. The molar MMC content of BSA-G-MMC was equal to the decrease in the number of free amino groups. On the other hand, the acylation of BSA with glutaric anhydride caused a significant decrease in the number of free amino groups. One mole of G-BSA and G-BSA-MMC showed the color intensity of only 1.2 and 1.5 mol of free amino groups, respectively.

1.3.2. Molecular weight

The molecular weights of the conjugates were determined by SDS–PAGE (Fig. 1). The samples were

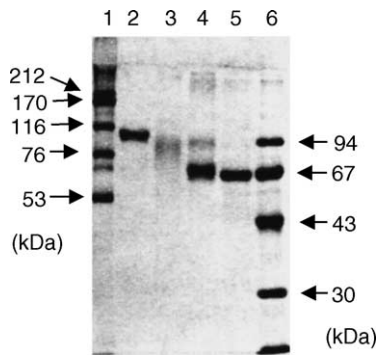

Fig. 1. SDS–PAGE of G-BSA (lane 2), G-BSA-MMC (lane 3), BSA-G-MMC (lane 4) and BSA (lane 5) (Tanaka et al., 1991). Aliquots of the sample were dissolved in the SDS-gel loading buffer containing 5% mercaptoethanol, heat-denatured, and loaded on the gel. After electrophoresis, the gel was stained with Coomassie Brilliant Blue. Line 1 and lane 6 show the migration patterns for the standard proteins.

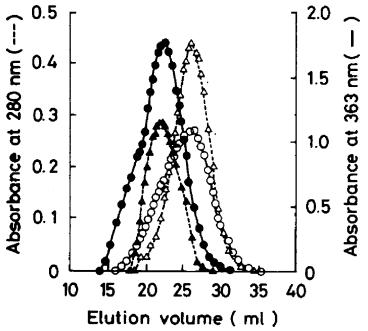

Fig. 2. Elution profiles of G-BSA-MMC (closed circle), G-BSA (closed triangle), BSA-G-MMC (open circle) and BSA (open triangle) (Tanaka et al., 1991). Size-exclusion chromatography was carried out on a Sephadex G-150 column (1.0 cm × 47 cm) with 0.2 M NaCl at room temperature. G-BSA-MMC and BSA-G-MMC were spectrophotometrically detected at 363 nm, whereas G-BSA and BSA were detected at 280 nm.

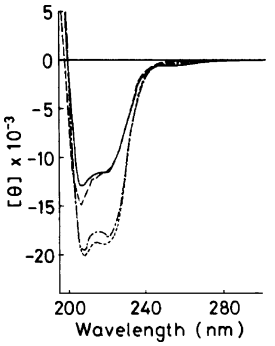

Fig. 3. Circular dichroism spectra of G-BSA-MMC (solid line), BSA-G-MMC (dot-dash line), G-BSA (broken line) and BSA (dotted line) (Tanaka et al., 1991). Each spectrum was recorded in a 0.1 mm path length cell on a JASCO J-20C spectropolarimeter equipped with a J-DPZ data processor.

treated with 2% SDS at 100 °C for 3 min prior to the gel electrophoresis. The molecular weights of both G-BSA-MMC and G-BSA were estimated to be somewhat larger than that of BSA by this method (Table 1).

1.3.3. Molecular size

The effective molecular sizes of the conjugates were determined by size-exclusion chromatography (Fig. 2). The elution volumes of G-BSA-MMC and G-BSA were smaller than that of BSA, indicating a significant increase in the Stokes radius (Table 1). BSA-G-MMC showed, however, a small increase in the molecular size compared to that of BSA.

1.3.4. Helical contents

Fig. 3 shows the CD spectra of the conjugates. Each spectrum consists of two negative dichroic hands located at 222 and 208 mm, respectively, and a crossover point at 200–201 nm indicating the presence of a right-handed α-helical structure. Table 1 shows the estimated helical content of the conjugates. Both BSA-G-MMC and BSA contained ca. 50% of helical content. However, G-BSA-MMC and G-BSA had significant low values of helical content under the same conditions.

1.3.5. Stability and release

The degradation of the conjugates was investigated in aqueous phosphate buffer solutions. The release of MMC was observed during the degradation of the conjugate at the pH range of 5.0–9.0. G-MMC was entirely undetected, however, in the experimental medium. The disappearance of both G-BSA-MMC and BSA-G-MMC in buffered solutions followed pseudo-first-order kinetics. The degradation of MMC at each pH followed apparent first-order kinetics, as did that of the conjugates.

On the basis of the present results, the overall reactions maybe described by Scheme 1, where k_1, k_2, and k_3 are apparent first-order rate constants for the depicted reactions. Thus, the concentration of the conjugate ([CONJUGATE]) and that of MMC released ([MMC]) in the buffered solution have a time dependence given by the following equations:

$$[\text{CONJUGATE}] = [\text{CONJUGATE}]_0 \times \exp(-(k_2 + k_3)t) \quad (1)$$

$$[\text{MMC}] = \frac{-k_2[\text{MMC}]_0}{(k_1 - (k_2 + k_3))} \times (\exp(-(k_2 + k_3)t) - \exp(-k_1 t)) \quad (2)$$

where [CONJUGATE] and $[\text{MMC}]_0$ represent the initial concentration of the conjugate and that of MMC covalently bound to the conjugate, respectively.

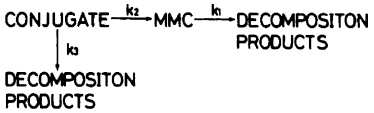

Scheme 1.

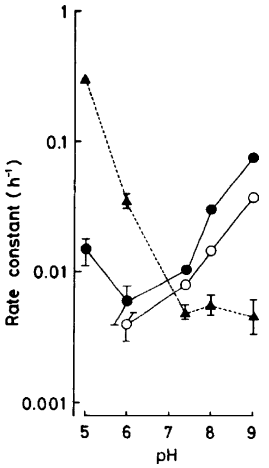

Fig. 4. pH profiles of the rate constants in the formation of MMC from the conjugates (k_2) and the degradation of MMC (k_1) in 0.1 M phosphate buffer solutions ($\mu = 0.3$) at 37 °C (Tanaka et al., 1991). Closed circle, G-BSA-MMC; open circle, BSA-G-MMC; closed triangle, MMC. Vertical bar represent S.D. calculated from 15 to 20 sets of experimental data by the least-squares method.

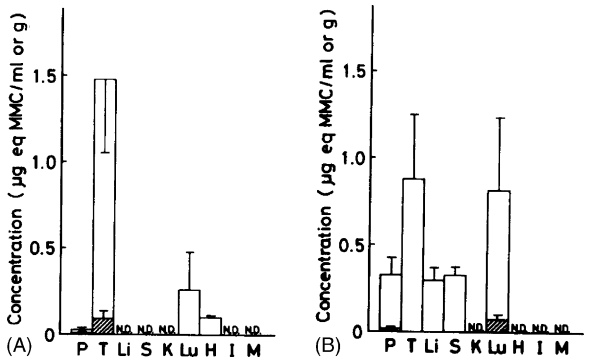

Fig. 5. Tissue distribution of the conjugate (open column) and the released MMC (slant lines column) in mice-bearing Ehrlich ascites cacinoma (EAC) cells 24 h after a single intravenous injection of G-BSA-MMC (A) and BSA-G-MMC (B) (Tanaka et al., 1991). The EAC cells (1×10^7 cells/mouse) were inoculated subcutaneously, and 14 days later each conjugate (20 mg/kg in MMC equivalents) was administered. Results are expressed as the mean ± S.D. of three mice. Key: P, plasma; T, tumor; L, liver; S, spleen; K, kidney; Lu, lung; H, heart; I, intestine; M, muscle; ND, not detectable.

Based on these equations, curve fitting was done by using the nonlinear-least-squares program MULTI (Yamaoka et al., 1981). The values of k_1 and k_2 showed good convergence. The degradation of MMC bound to the conjugate was regarded as negligible ($k_3 \neq 0$) because a small negative value of k_3 with an extraordinarily large standard deviation was obtained.

The pH-rate profiles of k_1 and k_2 are shown in Fig. 4. MMC was very stable above neutral pH, but decomposition increased markedly under acidic conditions (k_1, Fig. 4). Both G-BSA-MMC and BSA-G-MMC were relatively stable at low pH contrary to the findings with MMC, but they predominantly release MMC at pH 9.0 (k_2, Fig. 4). These results were similar to those obtained in the experiment of the MMC-asialofetuin conjugate (Kaneo et al., 1991).

Half-lives of the release of MMC from G-BSA-MMC and BSA-G-MMC under specific physiological conditions (pH 7.4 and 37 °C) were 66.0 and 84.0 h, respectively.

1.3.6. Disposition

Sustained concentrations of MMC after injection of the conjugates were observed in spite of the rapid elimination of MMC (data not shown). Higher and continuous levels of MMC were established especially by the administration of G-BSA-MMC. These conjugates appeared to release MMC continuously in the rats.

Fig. 5 shows the tissue distribution of MMC 24 h after a single intravenous injection of 20 mg/kg in MMC equivalents of the conjugates. Although free and conjugated forms of MMC were detected separately, most of MMC was detected as the conjugated form in the tissues. Both the conjugates may accumulated in the tumor tissues. G-BSA-MMC was distributed to the lung and the heart to some extent, and trace amounts of the conjugate were detected in the plasma (Fig. 5A). BSA-G-MMC accumulated not only in the tumor tissue but also in tissues such as liver, spleen, and lung (Fig. 5B). Significant amounts of BSA-G-MMC remained in the circulation even after 24 h. The concentration ratios of the tumor against the plasma were 62 and 2.8 for G-BSA-MMC and BSA-G-MMC, respectively.

1.3.7. In vivo antitumor activity

Fig. 6 shows the growth inhibition curves against S180 subcutaneously inoculated in mice. In the control, a remarkable tumor growth was observed, showing an 80 times increase in the ratio of the tumor volume after 30 days. A marked growth inhibition was achieved by a single dose of each conjugate; the

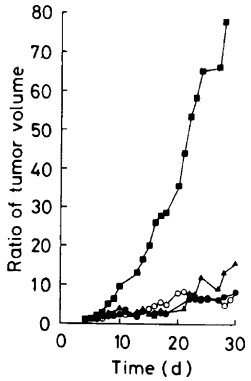

Fig. 6. Growth inhibitory effects of G-BSA-MMC, BSA-G-MMC and MMC on implanted S180 cells (Tanaka et al., 1991). Mice were inoculated with S180 cells (1×10^7 cells/mouse) subcutaneously. Four days after the inoculation, a single intravenous dose of the test compound was as follows: closed circle, G-BSA-MMC (20 mg/kg in MMC equivalents); open circle, BSA-G-MMC (20 mg/kg in MMC equivalents); closed triangle, MMC (5 mg/kg); closed square, control (0.9% NaCl, 10 ml/kg). The ratio was calculated by dividing the tumor volume by the reference volume 4 days after the inoculation. Each point represents the mean value of the ratio ($n = 6$–27).

ratios of tumor volume were kept at low values even 30 days after inoculation. S180-bearing mice (control) exhibited a survival ratio of 39% 40 days after inoculation. By the treatment with G-BSA-MMC and BSA-G-MMC (20 mg/kg in MMC equivalents) the 40-day survival ratio increased to 75 and 100%, respectively. Similarly, an improvement of the 40-day survival ratio was observed in the mice treated with MMC (5 mg/kg).

1.3.8. Acute toxicity

Acute intravenous LD_{50} values were determined by Dixon's up-and-down method. All animals were observed for 7 days after treatment. The LD_{50} values of G-BSA-MMC, BSA-G-MMC, and MMC were 51.1 mg/kg in MMC equivalents, 67.3 mg/kg in MMC equivalents, and 11.1 mg/kg, respectively. Severe weight loss and diarrhea observed above the dose of LD_{50}.

1.4. Discussion

A total of 60 mol of free amino groups (provided by the lysyl side chains and the single amino terminus) per mol of BSA has been determined by amino acid analysis and its primary sequence (Reed et al., 1980). In the case of BSA-G-MMC 5.6 mol of free amino groups of the BSA were modified by the binding of MMC. The number of the modified amino groups was identical with the MMC content of BSA-G-MMC (Table 1). One mole of BSA showed the color development comparable to that of 28.5 mol free amino groups according to the TNBS method. The extent of acylation of BSA by glutaric anhydride could not be estimated adequately by the colorimetric method. It was found, however, that G-BSA and G-BSA-MMC had only 1–2 mol reactive lysine residues on the molecular surface of BSA (Table 1). Kato and co-workers have prepared an albumin conjugate of MMC (BSA-MMC, 5.0 MMC/w (%)) by binding MMC directly to BSA using large amount of calbodiimide (Kato et al., 1982). The effective molecular size of BSA-MMC they made (99 Å) was much larger than that of BSA (34.4 Å). BSA is really polymerized during the carbodiimide reaction because it has both carboxyl and amino groups in its molecule. The prior acylation of BSA was found to prevent the protein polymerization in the presence of carbodiimide since the estimated molecular weight of G-BSA-MMC (84 kDa) was similar to that of BSA (68 kDa) (Table 1). Thus, G-BSA-MMC prepared in this study showed a much smaller Stokes radius (45.1 Å) according to the size exclusion chromatography on a Sephadex G-150 column (Table 1). On the other hand, the synthetic method of preparing G-MMC followed by binding to BSA (Method 2) did not influence the effective molecular size or the molecular weight of BSA (Table 1).

Acylation, such as acetylation and succinylation, have been reported to cause conformational changes of the protein which are attributed to an electrostatic destabilization (Habeeb, 1967). Glutarylation also resulted in a 30% increase in the Stokes radius of BSA (Table 1). Since a 40% decrease in the helical contents of G-BSA-MMC and G-BSA occurred, a partial unfolding and/or conformational change of the BSA molecule were suggested (Table 1). HPLC analysis showed that the conjugates did not release G-MMC but MMC directly. The conjugates were very stable at pH 6.0, contrary to the findings for MMC, but it predominantly released MMC with the elevation of pH. MMC was relatively stable at basic pH, but the

decomposition increased below neutral pH. These results were similar to those obtained in the experiment with an MMC-dextran conjugate (Hashida et al., 1983). Under the physiological conditions (pH 7.4 and 37 °C) BSA-MMC showed higher stability with a half-life of 84.0 h, comparing with G-BSA-MMC (66.0 h). The BSA-MMC conjugate synthesized by Kato et al. (1982) showed monoexponential release of MMC with a half-life of 20.2 h. The introduction of a glutaric spacer arm resulted in the slower release rate of MMC from the albumin conjugate. These findings indicate that covalent binding to BSA stabilizes MMC and that the macromolecular prodrugs, G-BSA-MMC and BSA-G-MMC liberate MMC gradually under the physiological conditions.

In rats, the α- and β-half-lives of free MMC given as MMC were 3.2 and 22.8 min, respectively. The elimination of the conjugated MMC from the plasma after dosing G-BSA-MMC and BSA-G-MMC was slower than that of free MMC given as MMC, with $t_{1/2}$ of 38.7 and 46.2 min, respectively. Since the plasma concentration–time profiles of free MMC after dosing the conjugates were not reconciled with the compartment model, the elimination parameters were calculated by the method of noncompartment model. The elimination half-lives of free MMC after administration of G-BSA-MMC and BSA-G-MMC were 8 and 2 h, respectively, and were much longer than that after dosing as MMC. Sustained levels of free MMC in the plasma suggested that the conjugates release MMC continuously in the body (Tanaka et al., 1991).

Macromolecules such as albumin, globulins, and synthetic polymers accumulate in the tumor tissues because of the unique vascular characteristics and a lack of the lymphatic recovery system (Matsumura and Maeda, 1986). We found that both G-BSA-MMC and BSA-G-MMC markedly accumulate in the tumor tissues in mice (Fig. 5A and B, respectively). Serum albumin is known to also distribute in the normal tissues including lung (Ghitescu et al., 1986). These findings may account for the high concentration of BSA-G-MMC in the lung (Fig. 5B) G-BSA-MMC, however; scarcely distributed to those normal tissues including lung, liver; and spleen (Fig. 5A). The characteristic distribution patterns of the conjugates were partly explicable by the difference of the higher structure such as molecular size and helical content (Table 1), because the pore radius of 40–58 Å was, for example, estimated for the pulmonary capillary membrane (Taylor and Gaar, 1970).

Effects of a single dose of 20 mg/kg in MMC equivalents of the conjugates on the growth inhibition of the tumor and on the survival ratio in S180-bearing mice were almost equivalent to those of a 5 mg/kg single dose of MMC (Fig. 6). MMC has severe side effects such as myelosuppression, gastrointestinal complications, and so on. In practice, the treatment with the conjugates did not result in necrosis of the site of injection nor severe diarrhea, which was observed by the treatment with MMC. These findings should account for the excellent efficiency of the conjugates compared to MMC.

The relative toxicities of the conjugates and MMC, as assessed by acute intravenous LD_{50} in the mice, were represented in order of decreasing potency by the following: MMC (11.1 mg/kg) ≫ G-BSA-MMC (51.1 mg/kg in MMC equivalents) > BSA-G-MMC (67.3 kg in MMC equivalents). The slow release rates of MMC from G-BSA-MMC and BSA-G-MMC may account for their lower acute toxicities compared to that of MMC.

These investigations showed that the albumin conjugates of MMC effectively accumulate in the tumor tissues and that the distribution of the conjugates depends on physicochemical properties such as molecular size.

2. Tumor targeting based on the mechanism of RME

2.1. Introduction

Targeting of drugs or toxins to tumor cells by specific carriers has long been a topic of interest. Macromolecules such as antibodies, glycoproteins, polysaccharides, and synthesized polymers have been candidates as carriers to tumor sites (Takakura and Hashida, 1995).

Transferrin (TF) is a glycoprotein which delivers iron ions to actively growing cells (De Jong et al., 1990). The high efficacy of the TF endocytosis process has tempted many investigators to ask whether this pathway could be exploited for the targeted delivery of drugs or larger molecules into cells

(Wagner et al., 1994). TF receptor levels in proliferating malignant cells have often been found to be far higher than in the corresponding normal cells. For this reason the TF receptor has been proposed as a target for cancer chemotherapy (Trowbridge, 1988).

Mitomycin C, which binds to DNA, is an antitumor antibiotic. Its use in chemotherapy is limited by severe side effects because it is distributed to normal cells as well as tumor cells. We synthesized a transferrin-mitomycin C conjugates and showed that the conjugates bound specifically to TF receptors on Sarcoma 180 cell (Tanaka et al., 1996). In this section, we describe the kinetics of the intracellular disposition of the conjugate in human leukemia cell line HL60 cells (Tanaka et al., 1998). And the efficiency of the conjugate as a receptor-mediated targeting system is discussed and its antitumor effect is also examined. Moreover, the binding and the internalization in the human hepatoma cell line HepG2 cell are discussed and compared with those in normal cultured hepatocyte (Tanaka et al., 2001).

2.2. Materials and methods

2.2.1. Materials

Human holo TF was obtained from Sigma Chemical Co. MMC, Eagle's minimum essential medium (Eagle), RPMI1640 and Dulbecco's minimum essential medium (Dulbecco's MEM) were purchased from Nacalai Tesque, Inc. Fetal bovine serum (FBS) was purchased from the Life Technologies (Gaithersburg, USA) and inactivated at 56 °C for 30 min before use. Collagenase (type H) was from Boehringer Mannheim (Tokyo, Japan). Percoll was purchased from Amersham Pharmacia Biotech (Tokyo, Japan). William's medium E was obtained from Dainippon Pharmaceutical Co., Ltd. (Suita, Japan). The conjugate of TF and MMC was synthesized according to the previous report (Tanaka et al., 1996). The conjugate or TF was labeled with ^{125}I (1 mCi, Amersham Corp., Tokyo, Japan) by the chloramine T method, in which the reaction time was limited to 1 min to avoid denaturation. Unbound ^{125}I was removed by chromatography on a column of PD-10 (Pharmacia Fine Chemicals). All other chemicals and reagents were of the highest grades commercially available.

2.2.2. Tumor cells

S180 cells were collected from the mice which were transplanted with S180 cells in the intraperitoneal cavity. The S180 cells were washed with Eagle supplemented with 1% BSA (BSA/Eagle).

HL60 cells were kindly supplied by Dr. Yamashita (Formulation Research Institute, Otsuka Pharmaceutical Co., Ltd., Tokushima, Japan) and grown in RPMI1640 supplemented with 10% PBS. Before the experiment, the cells were washed twice with ice-cold RPMI1640 supplemented with 1% bovine serum albumin (BSA/RPMI).

HepG2 cell was purchased from Riken Cell Bank (Wako, Japan). The HepG2 cells (5×10^5 cells) were plated in 35 mm plastic dishes in Dulbecco's MEM containing 10% PBS and were cultured in humidified air with 5% CO_2 at 37 °C. After 3 days, the cells were washed twice with ice-cold Dulbecco's MEM, supplemented with 1% bovine serum albumin (BSA/Dulbecco).

In order to wash out the endogenous TF, before the experiments the suspensions and/or the monolayer of the cells were incubated in the medium at 37 °C for 30 min and the cells were again washed twice with the medium.

2.2.3. Cultured hepatocyte

Hepatocytes were isolated from male Wistar rats by the collagenase perfusion method (Moldeus et al., 1978). The cells were fractionated on Percoll density gradients to obtain more than 98% viability as verified by the trypan blue exclusion test. Then the cells were resuspended in William's medium E containing dexamethasone (1 M), insulin (0.1 M), and 10% FBS. The cells (1×10^6 cells) were placed in a 35 mm collagen type I coated cultured dish (Iwaki, Funabashi, Japan) and cultured in humidified air with 5% CO_2 at 37 °C for 24 h. At the time of each experiment, the monolayers of hepatocytes were washed with Hanks medium, containing 1.3 mM $CaCl_2$ and 10 mM HEPES (pH 7.4), and incubated in 2 ml of William's medium E containing 1% BSA (BSA/William) at 37 °C for 30 min. Then the cells were again washed twice with ice-cold BSA/William.

2.2.4. Binding

S180 cells (5.0×10^6 cells) in BSA/Eagle were incubated with ^{125}I labeled ligands at 0 °C for 100 min.

HL60 cells (1.0×10^6 cells) in BSA/RPMI were incubated with ^{125}I labeled ligands at 0 °C for 100 min. After incubation, the cell suspension was added to an oil mixture (olive oil and dibutyl phthalate) and centrifuged at 5000 rpm for 2 min. A portion of the cell pellet was cut and the radioactivity of bound ^{125}I to the cells was determined with a gamma counter (Aloka301, Tokyo, Japan). ^{125}I labeled ligand was added to the washed monolayers of HepG2 cells and hepatocytes. The dishes were incubated at 0 °C for 100 min. The media were aspirated and the dishes were washed three times with ice-cold Hanks medium containing 1.3 mM $CaCl_2$ and 10 mM HEPES (pH 7.4). To correct nonspecific binding, assays were performed in parallel in the presence of 60 μM unlabeled TF.

2.2.5. Internalization

Internalization was started by the addition of ^{125}I labeled ligand to preincubated HL60 cells. The cell suspension (1×10^7 cells) in BSA/RPMI was incubated in the presence of 37.5 nM ^{125}I labeled ligand at 37 °C. The internalization was terminated by the addition of ice-cold BSA/RPMI to a portion of the incubation mixture. The cell suspension was centrifuged and then the cell pellet was washed three times with ice-cold BSA/RPMI. The radioactivity of the cell pellet was emitted by both bound and internalized ligand. In order to remove radioactivity from the cell surface, a portion of the incubation mixture was added to ice-cold 0.25 M acetic acid containing 0.5 M NaCl. The cell suspension was centrifuged and then the cell pellet was washed three times with an acidic solution. The radioactivity of the internalized ligand was determined in a gamma-counter. To the monolayers of HepG2 cells and hepatocytes, pre-warmed medium containing ^{125}I labeled ligand (9.4 nM) was added. Then the dishes were immediately placed at 37 °C. At the appropriate time, the dishes were washed three times with the ice-cold Hanks medium containing 1.3 mM $CaCl_2$ and 10 mM HEPES (pH 7.4). Another set of dishes similarly prepared was washed three times with ice-cold 0.25 M acetic acid containing 0.5 M NaCl to remove the cell surface binding ligand. In order to correct for nonspecific internalization, control experiments containing 60 μM unlabeled TF were run in parallel.

2.2.6. Recycling

Recycling of TF-MMC was studied according to the literature (Ciechanover et al., 1983) as follows. Washed HL60 cells (1×10^7 cells) were incubated with ^{125}I labeled ligand (37.5 nM) at 0 °C in BSA/RPMI for 100 min. Cells were rinsed with ice-cold BSA/RPMI to remove the unbound ligand. BSA/RPMI preheated at 37 °C was added to the cell pellet and reincubated at 37 °C for another 0, 2.5, 5, 7.5, 10, 15, 20, or 30 min. At the end of the incubation, cell mixtures were added to ice cold BSA/RPMI and centrifuged at 4 °C and 1000 rpm for 5 min. The radioactivities of the supernatant and the pellet were determined. Trichloroacetic acid (TCA) was added to the supernatant at a final concentration of 10% and the aliquot was centrifuged at 12,000 rpm for 10 min. The radioactivities of 10% TCA-soluble and insoluble fractions were measured. To distinguish the cell surface bound ligands from the internalized ligands, 0.25 M acetic acid/0.5 M NaCl was added to the cell pellet. The mixture was centrifuged at 4 °C and 1000 rpm for 5 min, and the radioactivity of the released ligands in the supernatant and the cell-associated counts were determined. In order to correct for a nonspecific endocytotic process, control experiments containing 60 μM unlabeled TF were run in parallel. In order to correct the intracellular disposition between TF-F-MMC and TF, we used a kinetic model which assumes that all of these process follow first-order kinetics (Scheme 2). The model consisted of the following steps: uptake of the ligand-TF-receptor complex into the cell (k_2); exocytosis of the ligand out of the cell (k_3); decomposition of the ligand (k_4); dissociation of the ligand from the ligand-TF receptor complex on the cell surface (k_1).

2.2.7. Cytotoxicity

Alamar Blue (Kanto Reagents, Tokyo, Japan) was used to determine cell proliferation. Briefly, HL60 cells (1×10^5 cells/ml) were inoculated into 96-well microplates (Nunc, Roskilde, Denmark). The cells were incubated with the test compound at specified

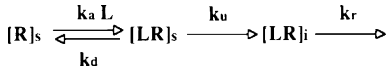

Scheme 2. Kinetic model of endocytosis of TF and TF-G-MMC.

concentrations in RPMI1640 containing 1% FBS at 37 °C for 3 days, followed by an additional 3-h incubation with Alamar Blue.

HepG2 cells (2×10^5 cells/ml) were inoculated in 96-well microplates (Nunc). The HepG2 cells were cultured in Dulbecco's MEM containing 2% FBS at 37 °C for 1 day. Isolated hepatocytes (2×10^5 cells/ml) were inoculated in collagen type I coated 96-well microplates (Iwaki) and cultured in the William's medium E containing dexamethasone (1 μM), insulin (0.1 μM), and 2% FBS at 37 °C for 1 day. The test compound at specified concentrations in the medium was added to the well and incubated at 37 °C for 2 days, followed by additional 3-h incubation with Alamar Blue.

The viable cell induces a chemical reduction of the Alamar Blue. The absorbance of reduced Alamar Blue was determined by a microplate reader (Immuno-mini, NJ-2300, Inter Med Japan, Tokyo, Japan). Growth inhibition (GI) was calculated using Eq. (3).

$$\mathrm{GI}\ (\%) = \left(1 - \frac{S - B}{C - B}\right) \times 100 \qquad (3)$$

where S, B and C represent the absorbance of the sample, the blank and the control, respectively.

2.3. Results

2.3.1. Preparation of the conjugate of MMC to TF (TF-G-MMC)

We have synthesized G-MMC by the method of Kato et al. (1983). The coupling of MMC to TF via a glutaryl group was achieved by using the active ester of MMC, 1α-[4-(*N*-succunumidoxycarbonyl)-butyl] mitomycin C (MMC-G-OSu) to provide covalent amide bonding. The MMC contents of the TF-G-MMCs are listed in Table 2. The MMC content of the conjugate increased with increasing amounts of MMC-G-OSu added to the reaction mixture.

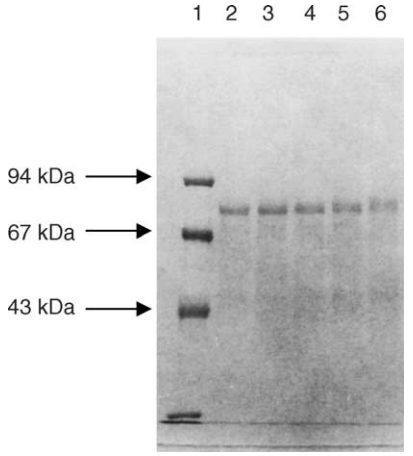

Fig. 7. SDS–PAGE of TF (lane 2) and TF-G-MMC with varying MMC content (lane 3: 0.82 MMC/w (%), lane 4: 1.80 MMC/w (%), lane 5: 4.04 MMC/w (%), lane 6: 9.49 MMC/w (%)) (Tanaka et al., 1996). Aliquots of the sample were dissolved in the SDS-gel loading buffer containing 5% of mereaptoethanol, then heat-denatured and loaded on the gel. After electrophoresis, the gel was stained with Coomassie Brilliant Blue. Lane 1 shows the migration patterns for the standard proteins.

The molecular weight of the conjugates was determined by SDS–PAGE (Fig. 7). The electromigration pattern of each TF-G-MMC was identified by a single band, thus TF did not aggregate to a polymeric form during the conjugation. The molecular weight of the conjugates was increased slightly by the conjugation of MMC (Table 2).

2.3.2. Binding of TF-MMC

2.3.2.1. Binding to the S180 cell. The equilibrium binding of TF and TF-G-MMC to S180 cell at 0 °C resulted in a saturation isotherm (Fig. 8). The

Table 2
Preparation and characterization of TF-G-MMC

Conjugate	Molar ratio of MMC-G-Osu/TF (mol/mol)	MMC content		Apparent molecular weight[a] (kDa)
		MMC/w (%)	Molar ratio	
1	4.3	0.82	1.97	81
2	8.7	1.80	4.32	82
3	22	4.04	9.70	83
4	43	9.49	22.8	84

[a] The apparent molecular weight was determined by SDS–PAGE.

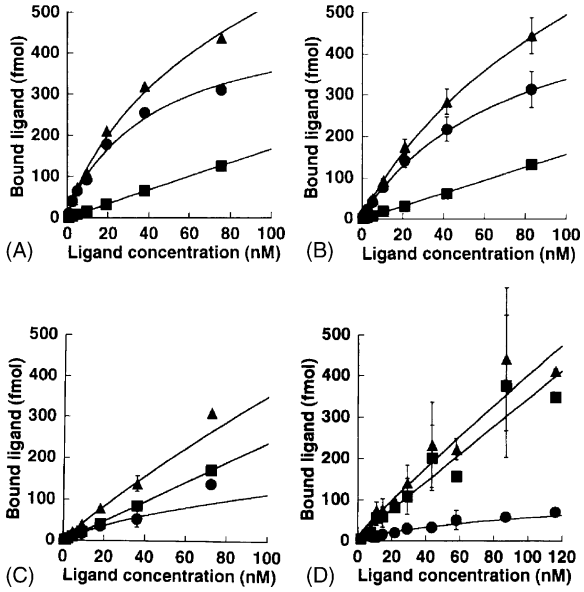

Fig. 8. Binding of ^{125}I-TF and ^{125}I-TF-G-MMC to Sarcoma 180 cells (4.0×10^6 cells) at pH 7.4 and 0 °C (Tanaka et al., 1996). (A) ^{125}I-TF; (B) ^{125}I-TF-G-MMC (0.82 MMC/w (%)); (C) ^{125}I-TF-G-MMC (4.04 MMC/w (%)); (D) ^{125}I-TF-G-MMC (9.49 MMC/w (%)). Specific binding (closed circle) is the mean of the difference obtained for total (closed triangle) and nonspecific (closed square) binding. Each line was calculated using the nonlinear least-squares program, MULTI.

Scatchard's plot of the data gave a nonlinear regression line (data not shown). Assuming that there are two types of binding sites, n_1 and n_2 with association constants K_1 and K_2, respectively:

$$B = \frac{n_1 K_1 L}{(1 + K_1 L)} + \frac{n_2 K_2 L}{(1 + K_2 L)} \quad (4)$$

where B and L represent the bound ligand concentration and the free ligand concentration, respectively. On the basis of Eq. (4), a curve fitting was done using the nonlinear least-squares program MULTI (Yamaoka et al., 1981). Table 3 lists the binding parameters obtained by computer analysis. For high-affinity TF-binding sites, the number (n_1) and the affinity constant (K_1) were 4500 sites/cell and $4.4 \times 10^8\ M^{-1}$, respectively. For low-affinity TF-binding sites, n_2 and K_2 were 72,000 sites/cell and $2.1 \times 10^7\ M^{-1}$, respectively.

Each equilibrium binding of TF-G-MMC with various MMC content resulted in a saturation isotherm (Fig. 8B–D). The total binding of the conjugate decreased as the MMC content increased. Nonspecific binding of the conjugate, which was determined in the presence of an excess amount of nonradioactive TF, increased as the MMC content was increased. Consequently, the specific binding of the conjugate to the TF receptor was depressed as the MMC content was increased. A Scatchard's plot of the specific binding data gave a nonlinear regression line (data not shown). The binding parameters of TF-G-MMC for the TF receptor on S180 cell are listed in Table 3. The numbers of binding sites (n_1 and n_2) of the conjugate 0.82 and 4.04 MMC/w (%) were nearly equal to those of TF; however, when the MMC content was increased to 9.49 MMC/w (%), n_1 and n_2 were decreased to one-half or one-third of those of TF, respectively.

2.3.2.2. Binding to the HL60 cell. The binding of TF-G-MMC (1.80 MMC/w (%)) was almost 50% of that of TF. The equilibrium binding of TF-G-MMC and TF resulted in a saturation isotherm. The

Table 3
Binding parameter[a] of TF and TF-G-MMC in the Sarcoma 180 cell at 0 °C

Compound	TF	TF-G-MMC		
MMC content (MMC/w (%))	–	0.820	4.04	9.49
n_1[b] (sites/cell)	4500	3600	5600	2200
K_1[c] (M^{-1})	4.4×10^8	1.2×10^8	3.7×10^8	1.3×10^8
n_2[b] (sites/cell)	72000	86000	55000	20000
K_2[c] (M^{-1})	2.1×10^7	1.2×10^7	3.0×10^6	4.7×10^6
Sum of nK (sites/cell M^{-1})	3.5×10^{12}	1.5×10^{12}	2.2×10^{12}	3.8×10^{11}

[a] Each parameter was calculated using the nonlinear least-squares program.
[b] The n_1 and n_2 are the number of the binding site.
[c] The K_1 and K_2 are the association constant. Each value is the mean ± S.D. which is calculated using a nonlinear least squares program, MULTI.

Table 4
Binding parameters of TF and TF-G-MMC (1.80 MMC/w (%)) in the HL60 cell, the HepG2 cell and the cultured hepatocyte[a] at 0 °C

Parameter	TF	TF-G-MMC
HL60 cell		
n[b] (sites/cell)	$2.58 \times 10^5 \pm 0.32 \times 10^5$	$1.16 \times 10^5 \pm 0.15 \times 10^5$
K[c] (M^{-1})	$1.16 \times 10^8 \pm 0.23 \times 10^8$	$1.45 \times 10^8 \pm 0.32 \times 10^8$
nK (sites/cell M^{-1})	3.0×10^{13}	1.7×10^{13}
HepG2 cell		
n[b] (sites/cell)	$4.11 \times 10^5 \pm 0.58 \times 10^5$	$3.96 \times 10^5 \pm 0.31 \times 10^5$
K[c] (M^{-1})	$4.50 \times 10^7 \pm 1.80 \times 10^7$	$3.24 \times 10^7 \pm 0.58 \times 10^7$
nK (sites/cell M^{-1})	1.8×10^{13}	1.3×10^{13}
Cultured hepatocyte		
n[b] (sites/cell)	$7.99 \times 10^3 \pm 2.14 \times 10^3$	$9.82 \times 10^3 \pm 2.06 \times 10^3$
K[c] (M^{-1})	$9.15 \times 10^7 \pm 7.38 \times 10^7$	$1.00 \times 10^5 \pm 0.65 \times 10^8$
nK (sites/cell M^{-1})	7.3×10^{11}	9.8×10^{11}

[a] This is the primary cultured rat hepatocyte.
[b] Number of the binding site.
[c] Association constant. Each value is the mean ± S.D. which is calculated using a nonlinear least squares program, MULTI.

Scatchard's plot of the data gave a linear regression line (data not shown). The binding parameters were calculated according to the following equation:

$$B = \frac{nKL}{(1 + KL)} \quad (5)$$

where B is the amount of bound ligand, n is the number of binding sites, K is the association constant and L is the free ligand concentration. Table 4 lists the binding parameter obtained by computer analysis.

2.3.2.3. Binding to the HepG2 cell and cultured hepatocyte. Cell surface binding of TF-G-MMC was compared with that of TF in monolayers of HepG2 cells and primary cultures of rat hepatocytes (data not shown). TF-G-MMC bound specifically to the HepG2 cell and hepatocyte as well as TF. These specific bindings resulted in saturation as the ligand concentration increased. Binding parameters were calculated according to Eq. (5). The binding parameters are listed in Table 4.

2.3.3. Internalization of TF-G-MMC

2.3.3.1. Internalization into the HL60 cell. 37.5 nM ^{125}I labeled ligands were incubated with HL60 cells at 37 °C (data not shown). The amount of surface binding of TF-G-MMC was maximal at 5 min after incubation. The amount of TF-G-MMC reached a maximum much faster than that of TF at 30 min. The maximal number of TF-G-MMC (0.715×10^5 molecules/cell) was almost 50% of that of TF (1.44×10 molecules/cell).

The amount of internalization of TF-G-MMC and TF increased with time and reached a steady-state within 20 min. However, the steady-state of internalization of TF-G-MMC was reached more slowly than that of TF. Experimental results for internalized ligands were fitted using Eq. (6):

$$I_t = I_{\mathrm{app,ss}}(1 - \mathrm{e}^{-k_{\mathrm{app,int}}}) \quad (6)$$

where I_t is the number of internalized ligand molecules per cell at time t, $I_{\mathrm{app,ss}}$ is the apparent steady-state level and is the apparent rate constant of internalization (Berczi et al., 1993). Table 5 lists the parameters obtained by computer analysis. Although the value of $I_{\mathrm{app,ss}}$ of TF-G-MMC was similar to that of TF, the rate constant of internalization of TF-G-MMC was smaller than that of TF.

2.3.3.2. Internalization into the HepG2 cell and cultured hepatocyte. TF-G-MMC and TF were incubated with the HepG2 cell and the cultured hepatocyte at 37 °C (Fig. 9). Each ligand was immediately bound to the cell surface. In the HepG2 cell, the amounts of binding of TF-G-MMC and TF reached the maximum value at 10 and 20 min, respectively. Then the amounts of binding were decreased gradually. In the hepatocyte, the amounts of binding of the ligands

Table 5
Kinetic parameters of internalization of TF and TF-G-MMC in the HL60 cell, the HepG2 cell and the cultured hepatocyte[a] at 37 °C

Parameter	TF	TF-G-MMC
HL60 cell		
$k_{app,int}$[b] (min^{-1})	0.213 ± 0.075	0.103 ± 0.021
$I_{app,ss}$[c] (molecules/cell)	$9.44 \times 10^4 \pm 0.83 \times 10^4$	$1.16 \times 10^5 \pm 0.09 \times 10^5$
HepG2 cell		
$k_{app,int}$[b] (min^{-1})	0.0707 ± 0.0112	0.0830 ± 0.0094
$I_{app,ss}$[c] (molecules/cell)	$1.79 \times 10^5 \pm 0.10 \times 10^5$	$1.04 \times 10^5 \pm 0.04 \times 10^5$
Cultured hepatocyte		
$k_{app,int}$[b] (min^{-1})	0.207 ± 0.056	0.132 ± 0.037
$I_{app,ss}$[c] (molecules/cell)	$0.239 \times 10^5 \pm 0.17 \times 10^5$	$0.224 \times 10^5 \pm 0.19 \times 10^5$

[a] This is the primary cultured rat hepatocyte.
[b] The apparent rate constant of internalization.
[c] The apparent steady-state level in the cell. Each value was calculated using a nonlinear least squares method.

reached the maximum at 5 min. The amounts of internalization were increased and reached an apparent steady-state level in both kinds of cells. The rate constants of internalization were calculated by Eq. (6).

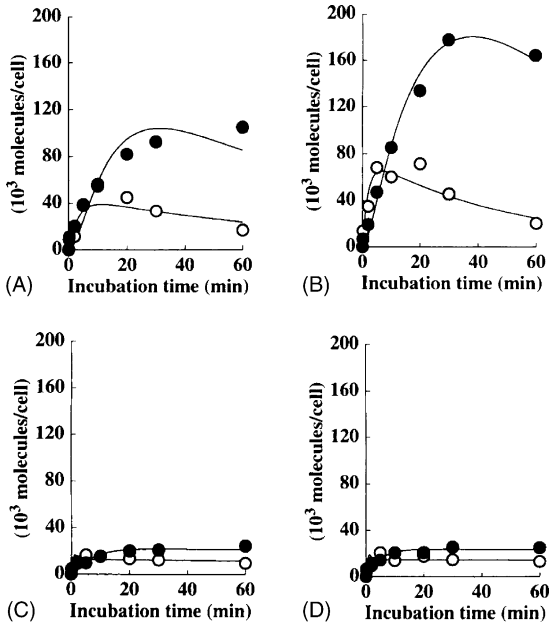

Fig. 9. Time profiles of binding (open circle) and internalization (closed circle) of [^{125}I]TF-MMC and [^{125}I]TF in the HepG2 cell and the cultured hepatocyte at 37 °C (Tanaka et al., 2001). (A) [^{125}I]TF-MMC in the HepG2 cell, (B) [^{125}I]TF in the HepG2 cell, (C) [^{125}I]TF-MMC in the hepatocyte, (D) [^{125}I]TF in the hepatocyte. Binding and internalization were simultaneously measured at the ligand concentration of 9.4 nM.

The parameters are listed in Table 5. In the HepG2 cell the apparent rates of internalization for TF-G-MMC and TF were almost equivalent; however; in the cultured hepatocyte the apparent rate for TF-G-MMC was slower than that for TF. The apparent rates of internalization for the ligands in the HepG2 cell were slightly slower than those in the cultured hepatocyte. The apparent steady-state levels of internalization in the HepG2 cell for the ligands were significantly higher than those in the cultured hepatocyte.

The rate of uptake into the cell and the rate of release from the cell were calculated according to the model of A.C. Myers et al. with a slight modification (Myers et al., 1987). Scheme 2 shows the kinetic model of endocytosis. The model is represented by three first-order differential equations as follows:

$$\frac{d[R]_s}{dt} = -k_a[L][R]_s + k_d[LR]_s \quad (7)$$

$$\frac{d[LR]_s}{dt} = k_a[L][R]_s - k_d[LR]_s - k_u[LR]_s \quad (8)$$

$$\frac{d[LR]_i}{dt} = k_u[LR]_s - k_r[LR]_i \quad (9)$$

where $[R]_s$ is number of the receptor on the cell surface, k_a is the rate constant of association. [L] is the ligand concentration, k_d is the rate constant of dissociation. $[LR]_s$ is the ligand-receptor complex on the cell surface, k_u is the rate constant of uptake, $[LR]_i$ is the ligand-receptor complex in the cell, and k_r is the rate constant of release from the cell. By solving those differential equations, $[LR]_s$ and $[LR]_i$ are expressed

Table 6
Kinetic parameters of endocytosis of TF and TF-G-MMC to the HepG2 cell and the cultured hepatocyte[a] at 37 °C

Cell type	TF	TF-G-MMC
$k_a[L]X_0$[b]		
HepG2 cell	$37.6 \times 10^3 \pm 9.7 \times 10^3$	$13.4 \times 10^3 \pm 7.1 \times 10^3$
Cultured hepatocyte	37.7×10^3[c]	$32.7 \times 10^3 \pm 13.9 \times 10^3$
α[b]		
HepG2 cell	0.506 ± 0.189	0.303 ± 0.207
Cultured hepatocyte	2.56[c]	2.51 ± 1.29
β[b]		
HepG2 cell	0.0189 ± 0.0067	0.0111 ± 0.0100
Cultured hepatocyte	0.000737[c]	0.00176 ± 0.00507
k_u[d]		
HepG2 cell	0.186 ± 0.037	0.277 ± 0.128
Cultured hepatocyte	0.365[c]	0.254 ± 0.101
k_r[e]		
HepG2 cell	0.0385 ± 0.0130	0.0862 ± 0.0525
Cultured hepatocyte	0.233[c]	0.144 ± 0.071

[a] This is the primary cultured rat hepatocyte.
[b] These parameters were defined in our report (Tanaka et al., 2001).
[c] The values were calculated using a nonlinear least squares algorithm, Simplex and the other values were calculated using a nonlinear least squares program, MULTI.
[d] The rate of uptake of the ligand-receptor complex into the cell.
[e] The rate of release of the ligand from the cell.

as equations as list in our report (Tanaka et al., 2001). The values of $k_{app,int}$ were used as the initial value in this model fitting. The lines in Fig. 9 represent the fitted curves by the MULTI using the model as shown in Scheme 2. Computer calculated parameters for the endocytosis of TF and TF-G-MMC are listed in Table 6.

2.3.4. Recycling of TF-G-MMC in the HL60 cell

In the recycling experiment of TF-G-MMC, the ratio of remaining radioactivity on the cell surface to the initially bound radioactivity decreased in time (Fig. 10). The internalized radioactivity was maximal at 7.5 min after incubation of 37 °C. At least 50% of the initial bound radioactivity was internalized within 7.5 min and then exocytosed. At 30 min, approximately 72% of the initially bound radioactivity was released from the cells. At that time, 9% of the initial bound radioactivity, which was not precipitable with 10% TCA, was released from the cells.

In the case of TF (Fig. 10B), the bound TF decreased in time. The ratio of internalization reached a maximum at 5 min and then decreased. The ratio of the released radioactivity was increased over time. At 30 min, 85% of the initial bound radioactivity, which was TCA-precipitable, was released from the cell. The TCA-soluble fraction was less than 1% of the initial bound radioactivity. Since TF was not decomposed

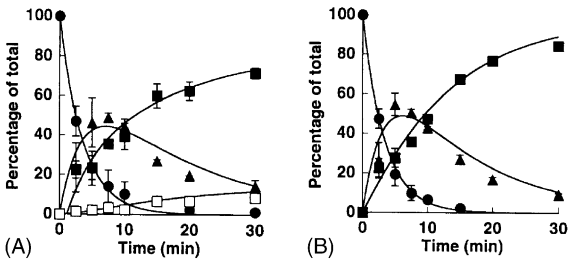

Fig. 10. Recycling experiments of [^{125}I]TF-MMC (A) and [^{125}I]TF (B) in HL60 cells at 37 °C (Tanaka et al., 1998). Each ligand (37.5 nM) was bound to a TF receptor on the cell surface at 0 °C for 100 min and the cells were washed with ice-cold BSA/RPMI. Then the cells were incubated at 37 °C and the radioactivity was analyzed (see Section 2). Closed circle, specific binding on the cell surface; closed triangle, remaining in the cell; closed square, TCA precipitable supernatant; open square, TCA-soluble. Each point and vertical bar represent the mean ± S.D. of two independent experiments. Each line represents computer-fitted profiles.

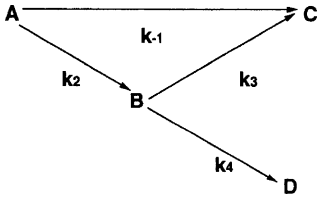

Scheme 3. Kinetic model of TF-MMC in the recycling experiment. A, amount of ligand on the cell surface; B, amount of ligand in the cell; C, amount of ligand out of the cell; D, amount of decomposed ligand; k_2, rate constant of uptake; k_3, rate constant of exocytosis; k_4, rate constant of decomposition; k_{-1}, dissociation of ligand from the ligand-TF-receptor complex on the cell surface.

to a TCA soluble compound, we considered a kinetic model which ignored the decomposition.

Kinetic parameters of the intracellular disposition of TF-G-MMC and TF were obtained by computer analysis according to the model of Scheme 3. The equations have been listed in our report (Tanaka et al., 1998). All the parameters were calculated by the least-squares program, MULTI (Yamaoka et al., 1981), and are listed in Table 7. As shown in Fig. 10, the simulated curves were in fair agreement with the experimental values.

2.3.5. Cytotoxicity of TF-G-MMC

2.3.5.1. Cytotoxicity against the HL60 cells. HL60 cells were incubated with different concentrations of TF-G-MMC (Fig. 11). The growth of HL60 cells was inhibited by the addition of TF-G-MMC and MMC. The growth inhibition of each compound showed a dose dependency. Concentrations resulting in the 50% inhibition of cell proliferation (IC_{50}) of TF-G-MMC and MMC were 1.6 μg MMC/ml and 0.41 μg/ml, respectively.

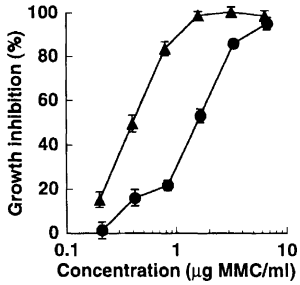

Fig. 11. Cytotoxicity of TF-MMC (closed circle) and MMC (closed triangle) against HL60 cells (Tanaka et al., 1998). The cells (1×10^5 cells/ml) were incubated with TF-MMC or MMC at 37 °C under 5% CO_2 air for 3 days. Each point and vertical bar represent the mean ± S.D. of three experiments.

2.3.5.2. Cytotoxicity against the HepG2 cell and cultured hepatocyte. HepG2 cells were incubated with different concentrations of TF-G-MMC and MMC (Fig. 12). Each compound inhibited the growth of the HepG2 cells. However, the relative viability of the hepatocytes was not changed by the addition of TF-G-MMC and MMC up to the concentration of 8 μg MMC/ml. Concentrations resulting in the 50% inhibition of cell proliferation (IC_{50}) of TF-G-MMC and MMC against the HepG2 cells were 0.9 μg MMC/ml and 0.5 μg/ml, respectively.

Table 7
Kinetic parameters of recycling of TF and TF-G-MMC in the HL 60 cell at 37 °C

Parameter	TF	TF-G-MMC
Rate constant[a] (min^{-1})		
k_{-1}	0.0641 ± 0.043	0.0915 ± 0.0090
k_2	0.231 ± 0.019	0.188 ± 0.015
k_3	0.0768 ± 0.0082	0.0453 ± 0.0055
k_4		0.0131 ± 0.0029
Mean time (min)		
Mean dissociation time (T_{-1})	15.6	10.9
Mean uptake time (T_2)	4.33	5.32
Mean exocytosis time (T_3)	13.0	22.1
Mean decomposition time (T_4)		76.3
Mean binding time (T_1 ($=T_{int} - T_2$))	1.13	1.82
Mean recycling time (T_5 ($=T_1 + T_2 + T_3$))	18.5	29.2

[a] Each value is the mean ± S.D. calculated using the MULTI.

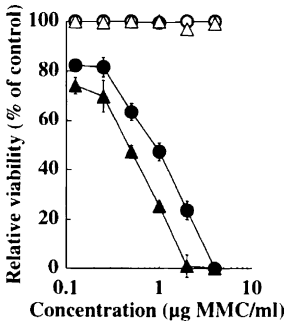

Fig. 12. Cytotoxicity of TF-MMC (circle) and MMC (triangle) against the HepG2 cells (closed symbols) and the cultured hepatocytes (open symbols) (Tanaka et al., 2001). The cells (1×10^5 cells/ml) were incubated with TF-MMC or MMC at 37 °C under 5% CO_2/air for 2 days.

2.4. Discussion

Targeting system to tumor cells has long been a topic of interest. TF has been considered a specific carrier of drugs, toxins, and DNA to tumor cells because the expression of a TF receptor has been well known to be increased in cells with malignant transformation (Hamilton et al., 1979). TF-G-MMC conjugates of differing molar ratios of MMC to TF were prepared. Up to a molar ratio of MMC-G-OSu/TF of 43, approximately half of the MMC-G-OSu added was attached to TF, and the conjugate was obtained in a good yield (>95.0% as protein). Above the molar ratio of 43, the yield of the conjugate was markedly decreased because of the formation of a water-insoluble product.

The biphasic curve obtained for the TF binding to the S180 cell was similar to the result of TF-binding analysis of the human adenocarcinoma cell line HT29-D4 (Roiron et al., 1989). On the other hand, Klausner et al. (1983) analyzed the binding of TF to human chronic myelogenous leukemia cell line K562 cell by assuming that the only one type of binding site is available. This discrepancy could be due to the fact that we used a more extensive range of ligand concentration. It has been suggested that the number of TF receptors in various malignant cell lines and cancerous tissues is increased compared with that in normal cells and tissues (Hamilton et al., 1979; Niitsu et al., 1987). For the sake of comparison with these binding parameters on the various kinds of cells, we used a sum of nK (e.g., $n_1K_1 + n_2K_2$). The sum of nK of TF on S180 cells, 3.5×10^{12} sites/cell M^{-1} was smaller than that on K562 (7.2×10^{13} sites/cell M^{-1}) (Klausner et al., 1983); however, it was larger than that on HT29-D4 (1.6×10^{12} sites/cell M^{-1}) (Roiron et al., 1989) and hepatocytes (5.9×10^{11} sites/cell M^{-1}) (Young and Aisen, 1980). These results indicated that TF was capable of binding to S180 cells more effectively than to normal cells. The number of total TF binding sites ($n_1 + n_2 = 76{,}500$ sites/cell) that we found on S180 cells was twofold larger than that on hepatocyte (37,700 sites/cell) (Young and Aisen, 1980). Therefore, TF would be a useful carrier for antitumor drugs to Sarcoma cell lines.

Each equilibrium binding of TF-G-MMC with various MMC content resulted in a saturation isotherm (Fig. 8B and D). The total binding of the TF-G-MMCs decreased as the MMC content increased. Nonspecific binding of the TF-G-MMC, which was determined in the presence of an excess amount of nonradioactive TF, increased as the MMC content increased. Consequently, the specific binding of the conjugate to the TF receptor was depressed as the MMC content was increased. A Scatchard's plot of the specific binding data gave a nonlinear regression line (data not shown). The binding parameters of TF-G-MMC for the TF receptor on S180 cells are listed in Table 2. The numbers of binding sites (n_1 and n_2) of the conjugate containing 0.82 and 4.04 MMC/w (%) were nearly equal to those of TF; however, when the MMC content was increased to 9.49 MMC/w (%), n_1 and n_2 were decreased to one-half or one-third of those of TF, respectively. The values of K_1 and K_2 decreased as the MMC content increased, e.g., TF-G-MMC containing 4.04 MMC/w (%) (10 mol MMC/mol TF) gave the value of K_2 which was one-seventh that of TF. These results indicate that the MMC content of the conjugate is an important factor with respect to the binding to the TF receptor.

In order to establish an effective tumor targeting system, we should conjugate MMC as much as possible to the TF molecule without losing the binding activity to the receptor. Table 3 shows the effect of the MMC content of TF-G-MMC on the sum of nK. The value of the sum of nK decreased as the MMC content increased. However, it was found that the conjugates with an MMC content below 10 mol MMC/mol TF retained more than half the activity of that of TF.

Moreover, we examined the binding of TF-G-MMC (1.80 MMC/w (%), 4 mol MMC/mol TF) and its antitumor activity against human leukemia HL60 cells. The conjugate was bound specifically to the TF receptor on the HL60 cells where the sum of *nK* was 1.7×10^{13} site/cell M^{-1}, and it exhibited an antitumor activity equivalent to that of MMC.

The binding affinity of TF to its receptor is influenced by ferric ion. At pH 7.2, the sum of *nK* of diferric TF (*holo*-transferrin) was 7.2×10^{13} and that of *apo*-transferrin was 3.2×10^{12} (Klausner et al., 1983). At both the N- and C-terminal regions of TF, the ferric ion was directly coordinated to two tyrosines, one histidine and one aspartic acid, and was indirectly coordinated to an arginine via the bicarbonate anion (Thorstensen and Romslo, 1990). The primary receptor-binding locus of human TF is thought to be in its C-terminal lobe, which contains glucosylated asparagines (MacGillivray et al., 1983), however, the N-terminal lobe enhances the binding of the C-terminal lobe (Zak et al., 1994). In the conjugation method using the active ester of glutarylated MMC, the drug linked randomly to the epsilon-amino groups of TF via the glutaryl spacer arm, since the 57 lysines are almost uniformly spread in the sequence (MacGillivray et al., 1983). Therefore, the chemical modification of TF with MMC might promote a conformational change in the TF molecule then indirectly affect the sites which were recognized by the TF receptor.

TF-G-MMC with an MMC content below 4.0 MMC/w (%) still retained more than half the activity of that of TF. Therefore, we examined the intracellular disposition of TF-G-MMC (1.8 MMC/w (%)), such as binding to the TF receptor, internalization, decomposition, and recycling in HL60 cells. TF-G-MMC (1.8 MMC/w (%)) bound specifically to the TF receptors on HL60 cells. The binding capacity of TF-G-MMC was less than half of that of TF at 0 °C (Table 4). At 37 °C, the amount of surface binding of TF-G-MMC and TF reached maximal levels after 5 and 30 min, respectively. The level of TF-G-MMC was almost that 50% of TF. It was suggested that the ratio of binding capacity of TF-G-MMC to TF was not altered under dynamic conditions. Over time, the amount of surface binding of the ligands decreased, indicating the down-regulation which occurs due to the stimulation of internalization.

The rate of internalization of TF-G-MMC is smaller than that of TF (Table 5). However, the value of $I_{app,ss}$ of TF-G-MMC (1.16×10^5 molecules/cell) is similar to that of TF (9.44×10^4 molecules/cell), indicating that the amount of the TF conjugate internalized in the steady-state was not changed with the chemical modification involving MMC.

Ciechanover et al. reported that the cycle of TF and its receptor in a cell takes place rather quickly, and the cycling time from the binding of *holo*-TF to the secretion of *apo*-TF takes about 16 min in HepG2 cell: on the average, about 4 min are required for the binding of *holo*-TF, 5 min for the internalization of a complex, 7 min for its return to the surface and 16 s for release of *apo*-TF into the medium (Ciechanover et al., 1983). In this study, the mean internalization time of TF was similar to that previously reported in HepG2 cells (Table 7). However, the recycling time of TF-G-MMC (29.2 min) is longer than that of TF (18.5 min), indicating that the chemical modification of TF influences its intracellular disposition. It was expected that the longer TF-MMC resides in the cell, the more cytotoxic TF-MMC becomes.

The extent of availability of endocytosis was calculated using Eq. (10):

$$F = \frac{\left(\int_0^\infty B\,\mathrm{d}t\right)_{\text{TF-G-MMC}}}{\left(\int_0^\infty B\,\mathrm{d}t\right)_{\text{TF}}} \tag{10}$$

where F is the extent of availability. In the recycling experiment, the value of F was 1.1, indicating that the extent of endocytosis of receptor-bound TF-G-MMC was almost similar to that of TF. Moreover, the $I_{app,ss}$ of TF-G-MMC is similar to that of TF. It is thought that the extent of availability of TF-G-MMC as a receptor-mediated targeting system is similar to that of TF.

The other factor involved in the cytotoxic effect of TF-MMC is a release of MMC from the conjugate. The recycling experiment showed that TF-G-MMC was internalized into the HL60 cell via the TF receptor, and a part of the internalized TF-G-MMC was decomposed into TCA-soluble fractions. The rate constant of the decomposition (k_4) was 0.0131 min^{-1}. The mean decomposition time (T_4) of TF-G-MMC was 76.3 min in the HL60 cell. We indicated that the release rate of MMC from the MMC-albumin conjugate was accelerated by the decomposition of the carrier protein

(Tanaka et al., 1995). The release rate of MMC from the TF-G-MMC might be accelerated after its internalization into HL60 cell.

The cytotoxicity of TF-G-MMC was examined in HL60 cells which were incubated with the conjugate at different concentrations. The values of the IC_{50} of TF-G-MMC and MMC were 1.6 μg MMC/ml and 0.41 μg/ml, respectively. This suggests that the TF-G-MMC has an inhibitory effect on the growth of HL60 cells.

The intracellular fate of TF-G-MMC is almost identical with TF, except for the degradation of TF-G-MMC. The intracellular fate of TF is well-known. TF binds to its receptor on the cell surface, the TF-receptor complexes are internalized in coated vesicles. The coated vesicles fuse with endosomes, an organelle with an internal pH of about 5–5.5 (Dautry-Varsat, 1986). TF-G-MMC might be susceptible to a weakly acidic condition. From the stability experiments, TF-G-MMC was released MMC at pH 5.0 (unpublished data). It is thought that the TF-G-MMC might act as a prodrug of MMC in HL60 cells. However, the release rate of MMC was too late to release MMC completely in the cell, if the release rate under the weakly acidic condition could increase, the conjugate might be particularly useful in combating the tumor cell. In an albumin conjugate of MMC, maleic acid and aconitic acid acted as a pH sensitive spacer arm which rapidly released MMC at pH 5.0 (Kaneo et al., 1990). Furthermore, poly-[*N*-(2-hydroxyethyl)-L-glutamine] conjugates of MMC, which used peptides as a spacer arm, released MMC rapidly at pH 5.5 and in the presence of lysosomal enzymes (De Marre et al., 1995). In this study, TF-G-MMC was degraded to a TCA soluble compound. This finding suggested that part of the internalized TF-G-MMC was delivered to lysosomes. The introduction of these pH sensitive spacer arms might make the TF conjugate of MMC a more effective antitumor prodrug.

Transferrin receptors were found to be more widely distributed on the tumor tissues than the normal tissues (Gatter et al., 1983). Transferrin can be exploited as a carrier of drugs, such as neocarzinostatin (Kohgo et al., 1990), adriamycin (Berczi et al., 1993), and cisplatin (Hoshino et al., 1995). We have described the covalent attachment of MMC to give TF-G-MMC, which aided the delivery of MMC to the tumor cells (Tanaka et al., 1996, 1998). Furthermore, we examined the intracellular disposition of TF-G-MMC, such as binding to the TF receptor and internalization in both the HepG2 cell and the cultured hepatocyte. By the calculation with MULTI, the number of the binding site (n) and the association constant (K) for TF-G-MMC were estimated to be 3.96×10^5 molecules/cell and $3.24 \times 10^7\ M^{-1}$, respectively (Table 5). The value of nK, which was used to compare the binding capacity of TF-G-MMC in the HepG2 cell, 1.3×10 molecules/cell M^{-1}, was almost equivalent to that of TF (1.8×10^{13} molecules/cell M^{-1}).

Ciechanover et al. reported that TF bound to the HepG2 cell with the value of nK of 1.2×10^{13} molecules/cell M^{-1} (Ciechanover et al., 1983). Our result of the value of nK of TF in the HepG2 cell was comparable to that of Ciechanover et al. We have reported that the conjugation of MMC to TF decreased the binding capacity to its receptor (Tanaka et al., 1996). In particular, the nonspecific binding of TF-G-MMC to the cell surface was affected by the conjugation of MMC with a high content. However, the nonspecific binding of TF to the cell surface did not change with the conjugation of MMC at the content of 1.8 w/w (%).

The binding parameters of TF have been evaluated in a variety of cells. Transferrin bound to the human erythroleukemia cell line K562 cell with the number of binding sites of 1.6×10^5 sites/cell and the value of nK of 7.2×10 molecules/cell M^{-1} (Klausner et al., 1983). We estimated the binding parameters to S180 cell (Tanaka et al., 1996) and the human leukemia cell line HL60 cell (Tanaka et al., 1998). The values of nK were 3.5×10 molecules/cell M^{-1} and 3.0×10 molecules/cell M^{-1}, respectively. Muller-Eberhard et al. (1988) examined the surface expression of the TF receptor in cultured rat hepatocyte. The hepatocyte exhibited a high affinity receptor for TF, in which the value of nK was 4.5×10^{11} molecules/cell M^{-1}. In our study, the values of nK of TF-MMC and TF in hepatocyte were 9.8×10^{11} molecules/cell M^{-1} and 7.3×10^{11} molecules/cell M^{-1}, respectively. Furthermore, TF bound to human reticulocyte with the value of nK of 7.5×10 molecules/cell M^{-1} (Frazier et al., 1982). These results represent that the TF receptor distributed to the tumor cells more than to the normal cells, such as hepatocyte and reticulocyte.

Our experiments demonstrated a pronounced difference in the intracellular disposition between the hepatoma cell line and the normal hepatocyte. TF-G-MMC bound significantly to the HepG2 cell surface by the TF receptor. In contrast to the HepG2 cell, the binding studies performed with the cultured hepatocyte showed that a little amount of TF-G-MMC bound specifically to the TF receptor. This difference indicates that TF-G-MMC is a useful drug targeting system for the HepG2 cell because the distribution of the TF receptor on the surface of the HepG2 cell is more than that of the normal hepatocyte.

At 37 °C, TF-G-MMC was bound to and internalized into both the HepG2 cell and hepatocyte (Fig. 9). In the HepG2 cell, the amount of surface binding of TF-G-MMC and TF reached maximal levels after 10 and 20 min, respectively. The maximal level of TF-G-MMC was 76% of TF. In the hepatocyte, the amount of surface binding of the ligands reached maximal levels which were almost equivalent in TF and TF-G-MMC. After the maximum point, the amount of surface binding of the ligands decreased, indicating the down-regulation occurred due to the stimulation of internalization. According to the sequential kinetic model as shown in Scheme 2, the rates of uptake of TF-G-MMC and TF in the HepG2 cell were almost identical to those in the hepatocyte (Table 6). The values of k_u for TF-G-MMC and TF in the HepG2 cell were $0.277 \pm 0.128\,min^{-1}$ and $0.186 \pm 0.037\,min^{-1}$, respectively. The values of k_u in the hepatocyte were $0.254 \pm 0.101\,min^{-1}$ and $0.265\,min^{-1}$, respectively. These values in the HepG2 cell and the hepatocyte were almost identical to those in the HL60 cell ($0.188 \pm 0.015\,min^{-1}$ for TF-G-MMC and $0.231 \pm 0.019\,min^{-1}$ for TF) (Tanaka et al., 1998). On the other hand, the rate of release of TF from the HL60 cell was $0.0768 \pm 0.0082\,min^{-1}$. In the HepG2 cell, the difference of the values of k_r between TF-G-MMC and TF was not detected. The values of k_r in the HepG2 cell were identical to that in the HL60 cell. However, the rates of release from the cell of TF-G-MMC and TF in the HepG2 cell were slower than those in the hepatocyte. The difference of k_r between the HepG2 cell and the hepatocyte might be one of the advantages for the tumor targeting system.

The AUC for internalization is derived by integration of $[LR]_i$ by time. In the HepG2 cell, the AUC for the internalization of TF-G-MMC and TF were 1.28×10^7 molecules min/cell and 1.90×10^7 molecules min/cell, respectively. In the hepatocyte, the AUC of TF-G-MMC and TF were 1.31×10^7 molecules min/cell and 6.46×10^7 molecules min/cell, respectively. The AUCs of the internalization of TF in each of the cells were slightly affected by the conjugation of MMC. The AUC of TF-G-MMC in the HepG2 cell was nearly identical to that in the hepatocyte. However, this study revealed that the level of TF-G-MMC internalized into the HepG2 cell was higher than that into the hepatocyte because the rate of release of TF-G-MMC from the HepG2 cell was slower than that from the hepatocyte. This indicates that the TF-G-MMC might be useful in delivering MMC into the HepG2 cell.

TF-G-MMC inhibited the growth of the HepG2 cells (Fig. 12). The IC_{50} of TF-G-MMC against the HepG2 cell was 0.9 g MMC/ml, which was a little higher than that of MMC ($IC_{50} = 0.5\,\mu g/ml$). MMC did not indicates cytotoxicity against the hepatocytes up to the concentration of 8 μg/ml. MMC reacts to the DNA during its replication and indicates cytotoxicity. Since the normal cultured hepatocyte does not divide in the in vitro condition, the viability of the hepatocytes did not change by the addition of MMC. TF-MMC also did not indicate cytotoxicity against the hepatocytes, not only because the cytotoxicity of MMC is specific to the dividing cell, but also because the level of internalization into the hepatocyte is low. TF-G-MMC and MMC have a cytotoxicity against the human leukemia cell line HL60 cell (Fig. 11) (Tanaka et al., 1998). The values of IC_{50} of MMC against the HepG2 cell and the HL60 cell were almost similar. However, TF-G-MMC was more cytotoxic against the HepG2 cell ($IC_{50} = 0.9\,\mu g$ MMC/ml, Fig. 12) than the HL60 cell ($IC_{50} = 1.6\,\mu g$ MMC/ml, Fig. 11). The level of internalization of TF-G-MMC in the HepG2 cell was larger than that in the HL60 cell. This may lead the TF-G-MMC to be more effective against the HepG2 cell than the HL60 cell. Faulk et al. have reported that TF-adriamycin conjugates inhibited redox and proton transport in the plasma membrane of K562 cells and killed these cells with greater efficiency than the free drug (Faulk et al., 1991). It can therefore be presumed that the cytotoxicity of TF-G-MMC against the HepG2 cells might be affected by the high binding affinity of TF-G-MMC to the cell.

These investigations showed that the TF-G-MMC was bound to and internalized into the HepG2 cell via the TF receptor. The rates of internalization of TF-G-MMC and TF into the HepG2 cell were nearly identical to those into the hepatocyte. However, the levels of the internalization into the HepG2 cell were remarkably higher than those into the hepatocyte because the number of receptors in the HepG2 cell was larger than that in the hepatocyte, and the rate of release of TF-G-MMC was slower than that of TF.

3. Conclusion

The study showed that the albumin conjugates of MMC effectively accumulate in the tumor tissues and that the distribution of the conjugates depends on physicochemical properties such as molecular size and conformation. The effect of EPR is useful for the passive targeting of the albumin-MMC prodrug. The tumor recognition by the mechanism of RME as an active targeting system needs an optimal chemical modification of the ligand. The optimum drug content gives the action as a tumor specific drug carrier system. The conjugate of MMC to TF (TF-G-MMC) was bound to the tumor cells and internalized via the TF receptor, and then a part of the internalized TF-G-MMC was degraded, suggesting that the release of MMC might represent antitumor activity. TF-G-MMC was demonstrated to be a useful hybrid as a receptor-mediated targeting system.

Control of the drug release from the conjugate and the intracellullar disposition of the drug will be the key point of the conquests of the further problems. The sensitivity against the pH of the organelle, such as endosome (pH = 5.0–5.5) and the protease in the lysosome would be one of the most important factors (Beyer et al., 2001; De Marre et al., 1995). And the other intelligence for the control of the intracellular disposition can be thought. It is a photochemical approach (Selbo et al., 2002), which would support the release of the antitumor drug from the conjugate. Further intelligence is needed to make the antitumor activity of the conjugate more effective.

Acknowledgements

This work was supported in part by a Grant-in-Aid for Scientific Research from the Ministry of Education, Science and Culture, Japan. The authors are grateful to Dr. Sato of Sasaki Laboratory and Dr. Yamashita of Otsuka Pharmaceutical Co. Ltd. for gifts of the tumor cell lines. The authors particularly acknowledge H. Kawashima, T. Sakaue, S. Yamano, N. Kitada, K. Shibaski, N. Ohira, Monden, Y. Yokota, A. Nakashima, M. Kato, and K. Imanishi for their technical assistance.

References

Berczi, A., Barabas, K., Sizensky, J.A., Faulk, W.P., 1993. Adriamycin conjugates of human transferrin bind transferrin receptors and kill K562 and HL60 cells. Arch. Biochem. Biophys. 300, 356–363.

Berczi, A., Ruthner, M., Szuts, V., Fritzer, M., Schweinzer, E., Goldenberg, H., 1993. Influence of conjugation of doxorubicin to transferrin on the iron uptake by K562 cells via receptor-mediated endocytosis. Eur. J. Biochem. 213, 427–436.

Beyer, U., Rothern-Rutishauser, B., Unger, C., Wunderli-Allenspach, H., Kratz, F., 2001. Differences in the intracellular distribution of acid-sensitive doxorubicin-protein conjugates in comparison to free and liposomal formulated doxorubicin as shown by confocal microscopy. Pharm. Res. 18, 29–38.

Chang, T.S., Sun, S.F., 1978. Structural studies on the succinylated bovine serum albumin. Int. J. Pept. Protein Res. 11, 65–72.

Ciechanover, A., Schwartz, A.L., Dautry-Varsat, A., Lodish, H.F., 1983. Kinetics of internalization and recycling of transferrin and the transferrin receptor in a human hepatoma cell line. J. Biol. Chem. 258, 9681–9689.

Ciechanover, A., Schwartz, A.L., Lodish, H.F., 1983. The asialoglycoprotein receptor internalizes and recycles independently of the transferrin and insulin receptors. Cell 32, 267–275.

Dautry-Varsat, A., 1986. Receptor-mediated endocytosis: the intracellular journey of transferrin and its receptor. Biochimie 68, 375–381.

De Jong, G., Van Dijk, J.P., Van Eijk, H.G., 1990. The biology of transferrin. Clin. Chim. Acta 190, 1–46.

De Marre, A., Soyez, H., Schacht, E., Shoaibi, M.A., Seymour, L.W., Rihova, B., 1995. Synthesis and evaluation of macromolecular prodrugs of mitomycin C. J. Control. Rel. 36, 87–97.

Dixon, W.J., 1965. The up-and-down method for small samples. J. Am. Statist. Assoc. 60, 967–978.

Faulk, W.P., Barabas, K., Sun, I.L., Crane, F.L., 1991. Transferrin-adriamycin conjugates which inhibit tumor cell proliferation without interaction with DNA inhibit plasma membrane oxidoreductase and proton release in K562 cells. Biochem. Int. 25, 815–822.

Fields, R., 1972. The rapid determination of amino groups with TNBS. Methods Enzymol. 25, 464–468.

Frazier, J.L., Caskey, J.H., Yoffe, M., Seligman, P.A., 1982. Studies of the transferrin receptor on both human reticulocytes and nucleated human cells in culture: comparison of factors regulating receptor density. J. Clin. Invest. 69, 853–865.

Friend, D.R., Pangburn, S., 1987. Site-specific drug delivery. Med. Res. Rev. 7, 53–106.

Gatter, K.C., Brown, G., Trowbridge, I.S., Woolston, R.E., Mason, D.Y., 1983. Transferrin receptors in human tissues: their distribution and possible clinical relevance. J. Clin. Pathol. 36, 539–545.

Ghitescu, L., Fixman, A., Simionescu, M., Simionescu, N., 1986. Specific binding sites for albumin restricted to plasmalemmal vesicles of continuous capillary endothielium: receptor-mediated transcytosis. J. Cell Biol. 102, 1304–1311.

Habeeb, A.F., 1967. Quantitation of conformational changes on chemical modification of proteins: use of succinylated proteins as a model. Arch. Biochem. Biophys. 121, 652–664.

Hamilton, T., Wada, H.G., Sussman, H.H., 1979. Identification of transferrin receptors on the surface of human cultured cells. Proc. Natl. Acad. Sci. U.S.A. 76, 6406–6410.

Hashida, M., Takakura, Y., Matsumoto, S., Sasaki, H., Kato, A., Kojima, T., Muranishi, S., Sezaki, H., 1983. Regeneration characteristics of mitomycin C-dextran conjugate in relation to its activity. Chem. Pharm. Bull. 31, 2055–2063.

Hoshino, T., Misaki, M., Yamamoto, M., Shimizu, H., Ogawa, Y., Toguchi, H., 1995. Receptor-binding, in vitro cytotoxicity, and in vivo distribution of transferrin-bound *cis*-platinum (II) of differing molar ratios. J. Control. Rel. 37, 75–81.

Kaneo, Y., Tanaka, T., Iguchi, S., 1990. Preparation and properties of mitomycin C-albumin conjugate. Chem. Pharm. Bull. 38, 2614–2616.

Kaneo, Y., Tanaka, T., Iguchi, S., 1991. Targeting of mitomycin C to the liver by the use of asialofetuin as a carrier. Chem. Pharm. Bull. 39, 999–1003.

Kato, A., Takakura, Y., Hashida, M., Kimura, T., Sezaki, H., 1982. Physico-chemical and antitumor characteristics of high molecular weight prodrugs of mitomycin C. Chem. Pharm. Bull. 30, 2951–2957.

Kato, Y., Tsukada, Y., Hara, T., Hirai, H., 1983. Enhanced antitumor activity of mitomycin C conjugated with anti-alpha-fetoprotein antibody by a novel method of conjugation. J. Appl. Biochem. 5, 313–319.

Klausner, R.D., Ashwell, G., Renswoude, J.V., Harford, J.B., Bridges, K.R., 1983. Binding of apotransferrin to K562 cells: explanation of the transferrin cycle. Proc. Natl. Acad. Sci. U.S.A. 80, 2263–2266.

Klausner, R.D., Renswoude, J.V., Ashwell, G., Kempf, C., Schechter, A.N., Dean, A., Bridges, K.R., 1983. Receptor-mediated endocytosis of transferrin in K562 cells. J. Biol. Chem. 258, 4715–4724.

Kohgo, Y., Kondo, H., Kato, J., Sasaki, K., Tsushima, N., Nishisato, T., Hirayama, M., Fujikawa, K., Shintani, N., Mogi, Y., Niitsu, Y., 1990. Kinetics of internalization and cytotoxicity of transferrin-neocarzinostatin conjugate in human leukemia cell line, K562. Jpn. J. Cancer Res. (Gann) 81, 91–99.

Laemmli, U.K., 1970. Cleavage of structural proteins during the assembly of the head of bacteriophage T4. Nature 227, 680–685.

MacGillivray, R.T.A., Mendez, E., Shewale, J.G., Sinha, S.K., Lineback-Zins, J., Brew, K., 1983. The primary structure of human serum transferrin. J. Biol. Chem. 258, 3543–3553.

Manabe, Y., Tsubota, T., Haruta, Y., Kataoka, K., Okazaki, M., Haisa, S., Nakamura, K., Kimura, I., 1985. Production of a monoclonal antibody-mitomycin C conjugate, utilizing dextran T-40, and its biological activity. Biochem. Pharmacol. 34, 289–291.

Matsumura, Y., Maeda, H., 1986. A new concept for macromolecular therapeutics in cancer chemotherapy: mechanism of tumoritropic accumulation of proteins and the antitumor agents Smancs. Cancer Res. 46, 6387–6392.

Moldeus, P., Hogberg, J., Orrenius, S., 1978. Isolation and use of liver cells. Methods Enzymol. 52, 60–71.

Muller-Eberhard, U., Liem, H.H., Grasso, J.A., Giffhorn-Katz, S., DeFalco, M.G., Katz, N.R., 1988. Increase in surface expression of transferrin receptors on cultured hepatocytes of adult rats in response to iron deficiency. J. Biol. Chem. 263, 14753–14756.

Myers, A.C., Kovach, J.S., Vuk-Pavlovic, S., 1987. Binding, internalization, and intracellular processing of protein ligands. J. Biol. Chem. 262, 6494–6499.

Niitsu, Y., Kohgo, Y., Nishisato, T., Kondo, H., Kato, J., Urushizaki, Y., Urushizaki, I., 1987. Transferrin receptors in human cancerous tissues. Tohoku J. Exp. Med. 153, 239–243.

Reed, R.G., Putnam, F.W., Peters Jr., T., 1980. Sequence of residues 400–403 of bovine serum albumin. Biochem. J. 191, 867–868.

Roiron, D., Amouric, M., Marvaldi, J., Figarella, C., 1989. Lactoferrin-binding sites as the surface of HT29-D4 cells. Comparison with transferrin. Eur. J. Biochem. 186, 367–373.

Roos, C.F., Matsumoto, S., Takakura, Y., Hashida, M., Sezaki, H., 1984. Physicochemical and antitumor characteristics of some polyamino acid prodrugs of mitomycin C. Int. J. Pharmaceut. 22, 75–87.

Selbo, P.K., Hogset, A., Prasmickaite, L., Berg, K., 2002. Photochemical internalisation: a novel drug delivery system. Tumour Biol. 23, 103–112.

Takakura, Y., Takagi, A., Hashida, M., Sezaki, H., 1987. Disposition and tumor localization of mitomycin C-dextran conjugates in mice. Pharm. Res. 4, 293–300.

Takakura, Y., Hashida, M., 1995. Macromolecular drug carrier systems in cancer chemotherapy: macromolecular prodrugs. Crit. Rev. Oncol. Hematol. 18, 207–231.

Tanaka, T., Kaneo, Y., Iguchi, S., 1991. Properties of mitomycin C-albumin conjugates in vitro and in vivo. Bioconjug. Chem. 2, 261–269.

Tanaka, T., Kaneo, Y., Miyashita, M., Shiramoto, S., 1995. Properties of water-insoluble mitomycin C-albumin conjugate as a sustained release drug delivery system in mice inoculated with Sarcoma 180. Biol. Pharm. Bull. 18, 1724–1728.

Tanaka, T., Kaneo, Y., Miyashita, M., 1996. Synthesis of transferrin-mitomycin C conjugate as a receptor-mediated drug targeting system. Biol. Pharm. Bull. 19, 774–777.

Tanaka, T., Kaneo, Y., Miyashita, M., 1998. Intracellular disposition and cytotoxicity of transferrin-mitomycin C conjugate in HL60 cells as a receptor-mediated drug targeting system. Biol. Pharm. Bull. 21, 147–152.

Tanaka, T., Fujishima, Y., Kaneo, Y., 2001. Receptor mediated endocytosis and cytotoxicity of transferrin-mitomycin C conjugate in the HepG2 cell and primary cultured rat hepatocyte. Biol. Pharm. Bull. 24, 268–273.

Taylor, A.E., Gaar Jr., K.A., 1970. Estimation of equivalent pore radii of pulmonary capillary and alveolar membranes. Am. J. Physiol. 218, 1133–1140.

Thorstensen, K., Romslo, I., 1990. The role of transferrin in the mechanism of cellular iron uptake. Biochem. J. 271, 1–10.

Trowbridge, I.S., 1988. Transferrin receptor as a potential therapeutic target. Prog. Allergy 45, 121–146.

Wagner, E., Curiel, D., Cotten, M., 1994. Delivery of drugs, proteins and genes into cells using transferrin as a ligand for receptor-mediated endocytosis. Adv. Drug Deliv. Rev. 14, 113–135.

Yamaoka, K., Tanigawara, Y., Nakagawa, T., Uno, T., 1981. A pharmacokinetic analysis program (MULTI) for microcomputer. J. Pharmaco-bio. Dyn. 4, 879–885.

Young, S.P., Aisen, P., 1980. The interaction of transferrin with isolated hepatocytes. Biochim. Biophys. Acta 633, 145–153.

Zak, O., Trinder, D., Aisen, P., 1994. Primary receptor-recognition site of human transferrin is in the C-terminal lobe. J. Biol. Chem. 269, 7110–7114.